Analysis of Saturn kilometric radiation near a source center

J. D. Menietti,[1] R. L. Mutel,[1] P. Schippers,[1] S.-Y. Ye,[1] D. A. Gurnett,[1] and L. Lamy[2]

Received 4 August 2011; revised 19 October 2011; accepted 21 October 2011; published 21 December 2011.

[1] The Cassini spacecraft flew very near a source region of Saturn kilometric radiation (SKR) on day 73 of 2008, the second known encounter with a source region at high latitude. The radio and plasma wave instrument, Radio and Plasma Wave Science, observed intense kilometric emission in the extraordinary X mode, ordinary O mode, and Z mode. The electron low-energy spectrometer obtained a phase space distribution of sufficient energy and pitch angle resolution to allow growth rate calculations. There is evidence of a shell-like electron plasma distribution that is unstable to the growth of SKR via the cyclotron maser instability. The growth rates calculated are adequate to explain the observed X and Z mode emission, but nonlinear effects are required to explain the large O mode gain (as is true for terrestrial observations). Narrowband emission, also present at the time, could also explain both the Z mode and the O mode. We present the results for comparison with a previously reported source region encounter and with similar observations at Earth auroral kilometric source regions.

Citation: Menietti, J. D., R. L. Mutel, P. Schippers, S.-Y. Ye, D. A. Gurnett, and L. Lamy (2011), Analysis of Saturn kilometric radiation near a source center, *J. Geophys. Res.*, *116*, A12222, doi:10.1029/2011JA017056.

1. Introduction

[2] Auroral radio emissions are observed at all the magnetized planets (Earth, Jupiter, Saturn, Uranus, and Neptune) [cf. *Zarka*, 1998]. The primary source of these radio emissions is believed to be the cyclotron maser instability (CMI) [*Wu and Lee*, 1979]. The free energy source has more recently been identified as trapped electrons [*Louarn and LeQueau*, 1996] and electron shell or horseshoe distributions with energies in the range 1 to 10 keV [*Delory et al.*, 1998; *Su et al.*, 2007]. The CMI as applied to terrestrial auroral kilometric radiation (AKR) has been articulated by *Wu and Lee* [1979] to explain emission occurring near the local cyclotron frequency, f_{ce}. The ratio of plasma frequency, f_p, to f_{ce} must be small ($\lesssim 0.3$). The emission propagates at large wave normal angle (between the wave vector and the magnetic field) primarily in the extraordinary (X) mode, but emission in the Z mode and ordinary mode (O) are also expected. The Z mode emission growth rates should be comparable to the X mode, while the ordinary mode emissions are expected to be at least two orders of magnitude lower for typical terrestrial AKR source regions with small plasma densities [cf. *Omidi et al.*, 1984; *Winglee*, 1985]. Observations of ordinary mode and Z mode in the auroral region have been reported in the past [*Gurnett et al.*, 1983; *Mellott et al.*, 1984; *Bahnsen et al.*, 1989]. All of the theoretical predictions for X mode have been confirmed by observations of the FAST satellite [cf. *Ergun et al.*, 1998], and by numerical simulations [cf. *Pritchett et al.*, 2002]. Recently, *Mutel et al.* [2010b] have reported high-resolution observations of the Cluster satellites very near the AKR source region that appear to distinguish Z mode and X mode emissions for the first time.

[3] While radio auroral emission has been observed from the magnetized planets and the CMI is generally accepted as the primary source of this emission, until recently only at Earth has the source region been directly observed by spacecraft. *Lamy et al.* [2010, 2011], *Kurth et al.* [2010], and *Schippers et al.* [2011] have recently reported observations within an auroral source region at Saturn. This encounter occurred on 17 October 2008 during a period when Cassini was at high orbital inclination, and surprisingly, was at a local time near midnight. The major source region of SKR is known to be in the morning-to-noon sector [cf. *Warwick et al.*, 1981; *Lamy et al.*, 2008].

[4] The Cassini spacecraft flew a series of orbits at high inclination and latitudes during 2008. These orbits had periapses over the southern poleward regions of Saturn from approximately 4 Saturn radii (R_s = 60,268 km). Saturn Kilometric Radiation (SKR) is observed typically in the frequency range from ~30 kHz to ~1 MHz, but rarely at frequencies as low as 5 kHz, which would require source regions extending from near the surface to as high as 5 Rs. Encounters with SKR source regions were not to be expected at these altitudes except under unusual conditions such as periods of solar wind compression that are associated with SKR intensifications and extensions to lower frequency as explained in the work of *Kurth et al.* [2005], *Jackman et al.* [2009, 2010], and *Bunce et al.* [2010]. This was probably the case for the SKR source encounter reported by *Lamy et al.* [2010, 2011], *Kurth et al.* [2010], and *Mutel et al.* [2010a]. For the source encounter of 17 October, *Lamy et al.* [2011]

[1]Department of Physics and Astronomy, University of Iowa, Iowa City, Iowa, USA.
[2]LESIA, Observatoire de Paris, Université Paris Diderot, UPMC, CNRS, Meudon, France.

Copyright 2011 by the American Geophysical Union.
0148-0227/11/2011JA017056

also reported both X mode and weaker O mode emission, with no Z mode observed. *Mutel et al.* [2010a] have reported a calculation of the growth rate of the X mode SKR using electron phase space distributions measured in situ by the electron spectrometer (ELS) on board Cassini, reporting a shell-like distribution. The ELS data at the time had 2 s resolution pitch angle coverage of approximately $135° < \alpha < 180°$. These calculations confirmed the CMI as the likely source mechanism and agree generally with the terrestrial AKR observations of *Ergun et al.* [1998]. After an extensive search of the SKR data obtained by the Cassini RPWS, several other examples of SKR source region candidates were found, but only one with sufficient electron phase space density to warrant a serious investigation of wave growth, as reported by *Menietti et al.* [2010]. In the current paper we extend the study of *Menietti et al.* [2010] and *Mutel et al.* [2010a] by investigating the sources of Z mode and O mode observed in the SKR source region. We find there is evidence indicating that the X mode, O mode, and Z mode may all be generated within a common source region by the cyclotron maser instability. The observations at Saturn are compared to those associated with AKR source regions at Earth.

2. Instrumentation

[5] The Cassini Radio and Plasma Wave Science (RPWS) instrument measures oscillating electric fields over the frequency range 1 Hz to 16 MHz and magnetic fields in the range 1 Hz to 12 kHz [cf. *Gurnett et al.*, 2004]. The instrument uses 3 nearly orthogonal electric field antennas and 3 orthogonal magnetic search coil antennas, providing a direction-finding capability. There are 5 receiver systems, including a high-frequency receiver (HFR) covering 3.5 kHz to 16 MHz; a medium frequency receiver (MFR) covering 24 Hz to 12 kHz; a low-frequency receiver (LFR) covering 1 Hz to 26 Hz; a 5 channel waveform receiver operating in either a 1–26 Hz or 3 Hz to 2.5 kHz mode. The data examined in this study are measured by the LFR, MFR, and HFR. Measurements from the three electric antennas using the HFR allow the determination of the direction of arrival, the Poynting flux (S) and the polarization of a radio wave using the analytical inversion methods provided by *Cecconi and Zarka* [2005]. See also *Cecconi et al.* [2009] and *Fischer et al.* [2009] for further discussion of the polarization methods.

[6] The Cassini Plasma Spectrometer (CAPS) is composed of three sensors: the electron spectrometer (ELS), the ion beam spectrometer (IBS), and the ion mass spectrometer (IMS). Of importance in this study is the ELS that contains an 8 detector fan array in a single plane. Each detector has a $5.2° \times 20°$ field of view for a total in-plane field of view of 160°. A rotating platform allows up to 2π sr of sky to be monitored in approximately 3 min. The instrument measures electron energy from 0.6 to 28,250 eV over a period of 2 s with a resolution of $\delta E/E = 0.17$ [cf. *Young et al.*, 2004].

3. Observations

[7] In Figure 1a we present a frequency-time spectrogram of the RPWS plasma wave data for day 73 of 2008 between 02:00 and 06:00 Universal Time (UT). The frequency scale is logarithmic and the color bar indicates the electric field intensity. Intense SKR is seen throughout this interval extending from approximately 4 kHz to nearly 100 kHz, and apparently, extending below the local measured electron cyclotron frequency (shown by the white line), particularly in the interval from about 04:35 to 04:40. The SKR spectral densities are similar in intensity to those observed on 17 October 2008, as reported by *Lamy et al.* [2010]. It is this time period in which the satellite could be within the SKR source region since SKR is a gyroresonant emission, but the RPWS frequency resolution at this time is about 500 Hz near f = 5 kHz, and is therefore not sufficient to confirm that *f* is clearly less than f_c. In Figure 1b we present a higher-resolution plot of this time over the smaller time period and a linear frequency scale from 04:15 to 05:05. The SKR source region is near 04:35 to 04:40 where the emission appears to extend below the local cyclotron frequency.

[8] Figure 2a presents the apparent polarization results for a time period included in Figure 1a. See *Cecconi and Zarka* [2005], *Ye et al.* [2010], and *Fischer et al.* [2009] for a description of how the polarization measurements are obtained. Figure 2a shows, from top to bottom, Poynting flux, circular polarization, linear polarization, and total polarization. The results shown in Figure 2a are apparent polarization rather than actual polarization because only two of the three antennas of the RPWS instrument were available for polarization measurements at the time (two-antenna mode) [cf. *Cecconi and Zarka*, 2005; *Fischer et al.*, 2009; *Ye et al.*, 2010]. For this instrument mode it is assumed that the radio emission is perpendicular to the antenna plane and that the emission is incident on magnetometer-boom side of the antenna plane. For the time period of Figure 2a the angle between the antenna plane and the direction to the center of Saturn changes slowly from about 45° to about 30°, so that the antenna plane orientation is relatively constant and there are no apparent changes of polarization due to spacecraft orientation. As discussed in the work of *Ye et al.* [2010] the real polarization of a wave is determined by magnetoionic mode and wave normal angle (between **k** and **B**). The magnetoionic mode determines the polarization sense of a wave with respect to the local magnetic field at the source. In the absence of plasma effects, the circular polarization sense of a radio emission with respect to the wave vector **k** will remain the same after it leaves the source region [*Gurnett et al.*, 1988]. From the second panel of Figure 2a and referring also to the wave identifications in Figure 1a, the dominant mode is the X mode emission of the SKR above the cyclotron frequency. However, there is a rather narrow-banded left-handed emission that is identified as O mode at lowest frequencies above the cyclotron frequency. Below the cyclotron frequency is another narrow-banded emission with dominantly right-handed polarization that we identify as Z mode. These identifications follow from the fact that the satellite is in a low-density region with the ratio of plasma to cyclotron frequency being probably close to 0.046 as determined from the whistler mode cutoff frequency near 300 Hz (not shown). As discussed by *Gurnett et al.* [1983], auroral Z mode emission propagates in the frequency range $f_{L=0} < f < f_{UH}$, where $f_L = 0$ is the L = 0 cutoff given by $f_L = 0 = -\frac{f_c}{2} + \sqrt{\left(\frac{f_c}{2}\right)^2 + \left(f_p\right)^2}$. Since $f_{UH} = \sqrt{(f_c)^2 + \left(f_p\right)^2}$, and $f_p \ll f_c$, $f_{UH} \sim f_c$. As discussed in the

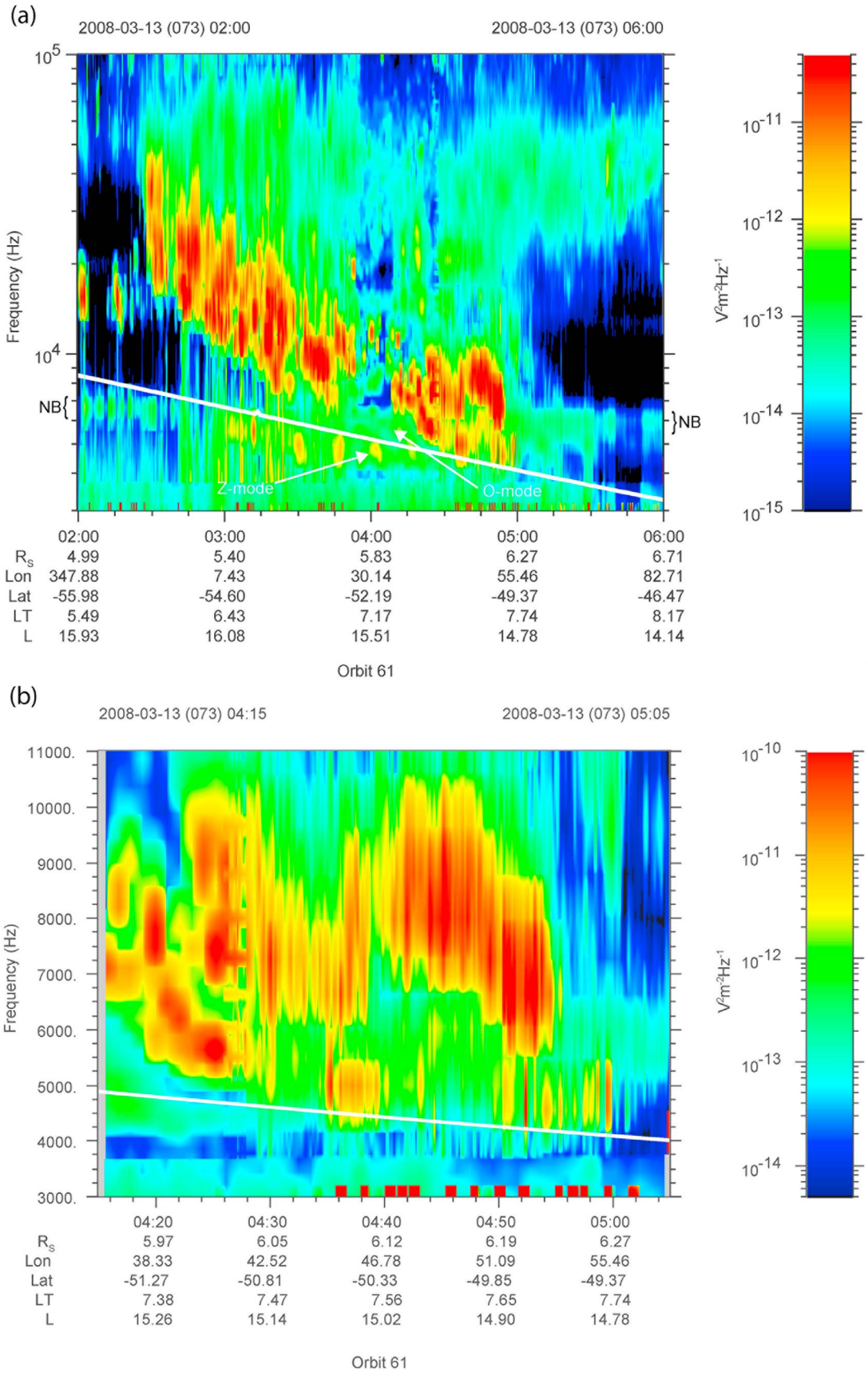
(a)
2008-03-13 (073) 02:00
2008-03-13 (073) 06:00
Frequency (Hz)
NB
NB
Z-mode
O-mode
02:00 03:00 04:00 05:00 06:00
R_S 4.99 5.40 5.83 6.27 6.71
Lon 347.88 7.43 30.14 55.46 82.71
Lat -55.98 -54.60 -52.19 -49.37 -46.47
LT 5.49 6.43 7.17 7.74 8.17
L 15.93 16.08 15.51 14.78 14.14
Orbit 61
V²m⁻²Hz⁻¹
(b)
2008-03-13 (073) 04:15
2008-03-13 (073) 05:05
Frequency (Hz)
04:20 04:30 04:40 04:50 05:00
R_S 5.97 6.05 6.12 6.19 6.27
Lon 38.33 42.52 46.78 51.09 55.46
Lat -51.27 -50.81 -50.33 -49.85 -49.37
LT 7.38 7.47 7.56 7.65 7.74
L 15.26 15.14 15.02 14.90 14.78
Orbit 61
V²m⁻²Hz⁻¹

Figure 1

work of *Benson et al.* [2006], for low-density regions ($f_p/f_c < 1$) this emission propagates in the R-X mode. The whistler mode upper cutoff frequency is either f_p or f_c, whichever is lower. Thus, the only two possible electromagnetic modes in the frequency range $f_p < f < f_{UH} \sim f_c$ are the O mode and the Z mode, which have opposite polarizations. The Z mode emission is not as highly polarized as O mode or X mode (fourth panel of Figure 2a), which may be due to the receivers adding the signals from both O mode and Z mode emission. This would be consistent with both O mode and Z mode propagating below f_{ce}. Between 04:30 and 05:00 UT note from the second panel of Figure 2a that SKR emission is in red shades (X mode) and extends down to f_{ce} (frequency resolution of ~500 Hz).

[9] Figure 1a indicates narrowband (NB) emission observed in the freely propagating L-O mode in the frequency range ~6 kHz < f < ~7.5 kHz. This emission, first reported at Saturn by *Gurnett et al.* [1981] from Voyager observations of the Plasma Wave Science instruments, has been discussed in detail by *Louarn et al.* [2007] and *Ye et al.* [2009] using Cassini RPWS observations. These emissions are observed in narrow, almost constant frequency bands near 5 kHz and also near 20 kHz and harmonics. The 5 kHz narrowband emission has been detected at all latitudes covered by the spacecraft, while the 20 kHz NB emission is only observed at relatively high latitudes [*Wang et al.*, 2010]. Recently, *Ye et al.* [2010] have reported intense NB emission in the Z mode for frequencies less than f_{ce}. *Ye et al.* [2010] propose that the narrowband emission is probably generated in the Z mode, while its L-O mode component may result from mode conversion of the original Z mode emission. The emission identified in Figure 1a and the second panel of Figure 2a as NB most likely has a source region distinct from the SKR emissions, which have a source region near the spacecraft in the time period ~04:35 to 04:40 UT for frequencies less than 5 kHz. In the second panel of Figure 2a (circular polarization) the NB emission is observed as Z mode emission for $f < f_{ce}$ and $t \lesssim$ 02:50 UT, while for $t \gtrsim$ 05:00 UT, NB emission is observed as L-O mode for $f > f_{ce}$. The frequency range of NB (~6 kHz < f < 7.5 kHz) does not change, but when the emission encounters the local cyclotron frequency, only L-O component of the emission can propagate for $f > f_{ce}$. We believe the NB emission has a remote source region and is propagating through the region containing magnetic field lines associated with the SKR source region.

[10] Mode conversion of Z mode to O mode emission takes place for small wave normal angles as discussed by *Jones* [1976], *Melrose* [1981], and *Ye et al.* [2009]. It is possible that the highly polarized O mode emission centered near 04:00 UT in the second panel of Figure 2a (blue color) could be NB emission that has mode converted from the Z mode emission at $f < f_{ce}$, but it may also be emission that has propagated from the nearby SKR source region near 04:39 UT. Figure 2b is a blow-up of the second panel of Figure 2a. The SKR source region is near the time interval 04:35 to 04:40 UT (hashed), and we have labeled probable emission modes near this time range.

[11] We have examined the electron phase space distribution (PSD) function from the ELS instrument for the time period from about 04:35 to 04:40 UT near the source region. During this time the instrument required several minutes to obtain a full range of pitch angle samples. However, this period of time is much longer than the growth period of SKR, and the electron distribution function observed after many seconds of time is relaxed owing to growth of the waves. To overcome this problem we chose an 8 s sampling period by averaging four successive measurements which provided the highest available time resolution of the PSD with continuous pitch angle coverage, but a very limited sampling of pitch angles. Rapid sampling times with a full pitch angle distribution as are now obtainable for terrestrial observations of auroral kilometric radiation are simply not available. In Figure 3 we display sampling of the PSD versus total velocity ($\sqrt{V_\parallel^2 + V_\perp^2}$) for a number of 8 s time intervals commencing at 04:35:44 UT. Each line represents data for a different anode (pitch angle), with the range indicated by the color code. Figures 3a–3c show increasing order in the data from multiple anodes. While there is scatter in the curves for each pitch angle, in Figure 3a note that there are a number of anodes (see caption for pitch angles) with intensity enhancements that occur near $4–6 \times 10^7$ m/s, indicating a shell-like distribution. As we show later the range $4 \lesssim V_{tot} \lesssim 6 \times 10^7$ m/s is close to the radius of the resonance ellipse for the local plasma parameters. Calculation of the growth rate for the CMI must be performed along the resonance ellipse. All anodes show some enhancement for $V_{tot} > 4 \times 10^7$ m/s except anode 1 for a pitch angle of 101.13° (lowest, black curve). Each panel of Figure 3 displays a different 8 s period, advancing in time through the SKR near-source region. The variability in the PSD among the anodes for $V_{tot} \lesssim 4.5 \times 10^7$ m/s in Figure 3a is probably due to temporal effects. In Figure 3b, for 04:36:08 UT, the PSD for 6 anodes shows an enhancement near $V_{tot} = 5 \times 10^7$ m/s, again indicating a shell-like distribution. In Figure 3c, for 04:38:56 UT, there is additional order in the observed distributions in the range $V_{tot} = 4$ to 6×10^7 m/s, showing more evidence of a shell-like distribution. Four of the anodes show very similar values in the range 4.25 to 5.25×10^7 m/s, and a repeating peak near 5×10^7 m/s. For $V_{tot} < 4 \times 10^7$, there is considerable scatter among the anodes with peaks occurring at no common value of V_{tot}. We have re-processed the data near this time for a 16-s interval as displayed in Figure 3d. Figure 3d shows similar curves and at least 4 anodes have a peak near 5×10^7 m/s, indicating the shell-like distribution persists for a time. The dotted curve is an average of the PSD values for those curves peaking near 5×10^7 m/s. We single out the green curve (anode 4, pitch angle of

Figure 1. (a) Frequency versus time spectrogram with color-coded electric field intensity. The frequency scale is logarithmic over the range 1–100 kHz. The white line indicates the local cyclotron frequency, f_c. Most of the emission above f_c is SKR. The intense emission below and close to f_c is likely Z mode with a mixture of less intense O mode. Narrowband (NB) emission, likely from a remote source, is also indicated. (b) Close-up view of the data in Figure 1a for a 50 min time interval plotted over a linear frequency scale from 3 to 11 kHz only. The region close to the SKR source is from about 04:35 to 04:40 UT, where the SKR X mode intensity appears to extend below f_c.

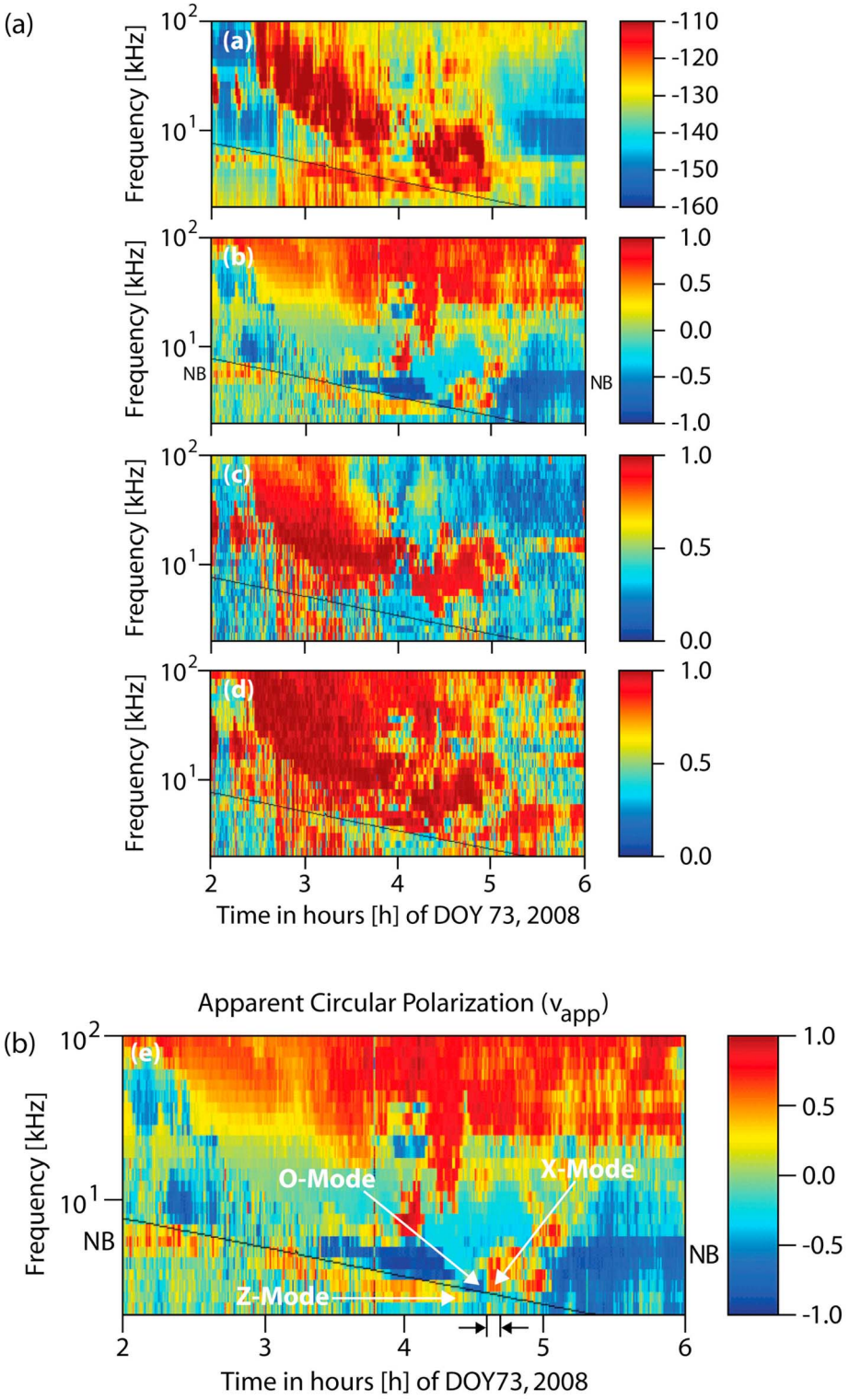

Figure 2. (a) Polarization results for 02:00 to 06:00 UT are displayed. From top to bottom: apparent Poynting flux, apparent circular polarization, apparent linear polarization, and apparent total polarization. The color bar for circular polarization is red for X mode and blue for O mode. For linear and total polarization the color bar is blue for 0% and red for 100%. The Poynting flux is displayed with a color bar in decibels. The black diagonal line indicates the cyclotron frequency. (b) An expanded version of apparent circular polarization in Figure 2a.

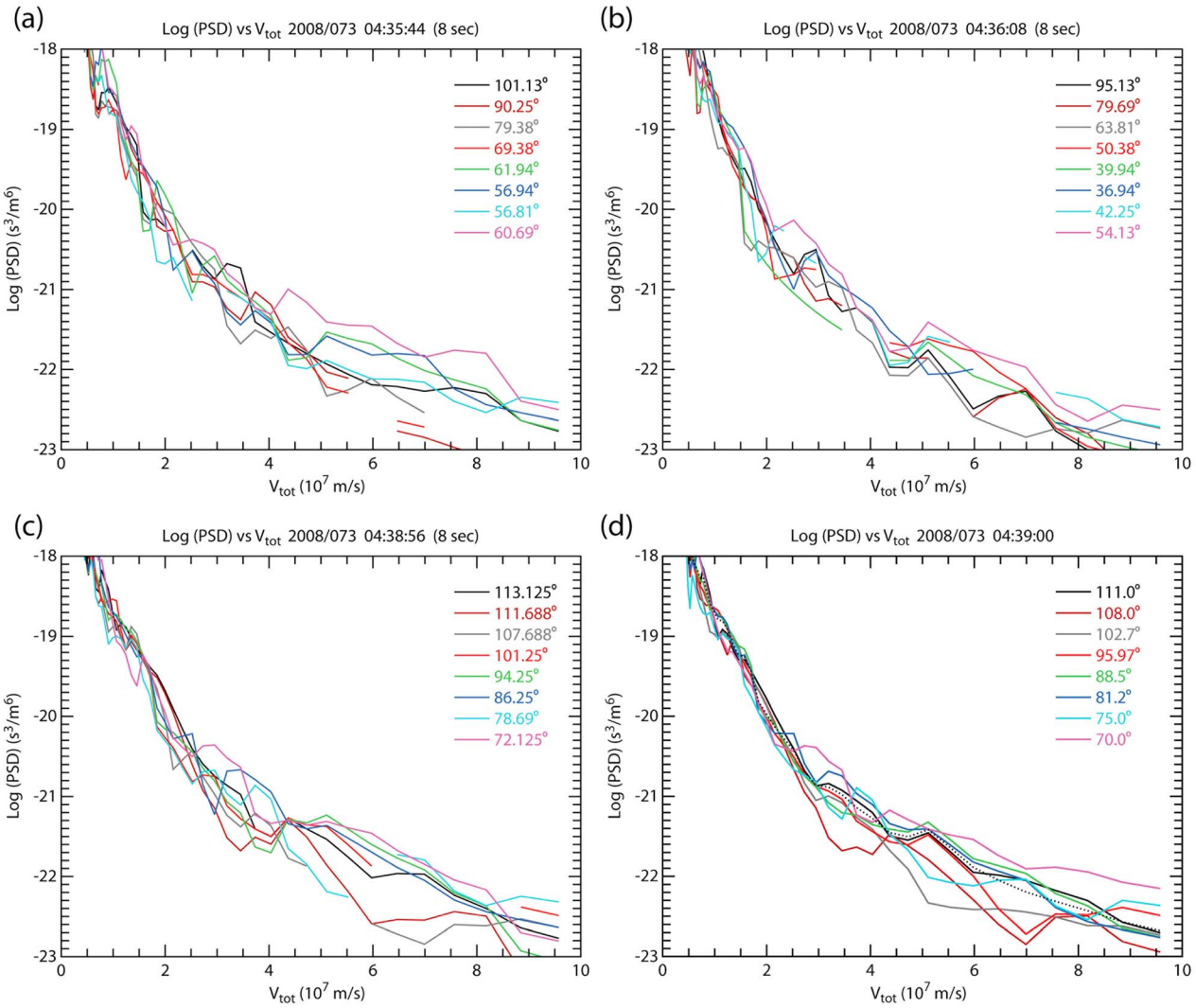

Figure 3. (a–c) Phase space density of electrons versus V_{tot} for each of the eight anodes (pitch angles) of the ELS instrument. Figures 3a–3c are averaged over 8 s, and each is for a different time period in the region nearest the SKR source region. The mean pitch angle for each anode is shown in the color key. Shown are enhancements for the range $4 < V_{tot} < 6 \times 10^7$ m/s, indicating a shell-like distribution. The organization of the data increases in Figures 3a–3c. (d) A 16 s average of the data included in Figure 3c. We single out the green curve (pitch angle of 88.5°) for modeling. The dotted line in Figure 3d is the average of the PSD for curves at pitch angles of 81.2°, 88.5°, 95.97°, and 111.0°.

88.5°) to model the shell-like distribution in order to perform wave growth calculations. This curve has a profile very similar to those of Figure 5c at the same energy. To model the distribution we use a Dory-Guest-Harris (DGH) [*Dory et al.*, 1965] analytical function given as

$$f(p) = \frac{n}{j!(2\pi)^{3/2} V_\perp^2 V_\parallel} \left(\frac{\nu_\perp^2}{2V_\perp^2}\right)^j \exp\left[-\frac{\nu_\perp^2}{2V_\perp^2} - \frac{(\nu_\parallel - U)^2}{2V_\parallel^2}\right] \quad (1)$$

where n is the number density of a plasma component, V is the thermal velocity, U is the drift velocity (which we assume to be 0), and $j \geq 0$ is an integer. Parallel and perpendicular are relative to the magnetic field. For $j = 0$ the distribution is a bi-Maxwellian. We have assumed both a cold core population ($j = 0$) and a warm component. In Figure 4 we plot the data for anode 4 (pitch angle = 88.5°, dashes) and the model DGH distribution for the warm component only (dot-dash). We have visually fit the distribution to the data. The warm component (keV electrons that provide the free energy for the CMI) has $n_\omega = 2.7 \times 10^{-4}$ cm^{-3}, $V_\parallel = 3.35 \times 10^7$ m/s, $V_\perp = 1.13 \times 10^7$ m/s, and $j = 11$, which places the center of a broad model shell distribution near 7.4 keV. The electron energy of 7.4 keV is somewhat smaller than that used by *Mutel et al.* [2010a] for the 17 October SKR source region, which was near 10 keV [cf. *Schippers et al.*, 2011].

[12] The total plasma density, n_e, is estimated by the upper cutoff frequency of the whistler mode emission which is close to 300 Hz (not shown). For $n_\omega = 2.7 \times 10^{-4}$ cm^{-3}, $n_\omega/n_e = 0.24$. This ratio is similar to that found for the 17 October source

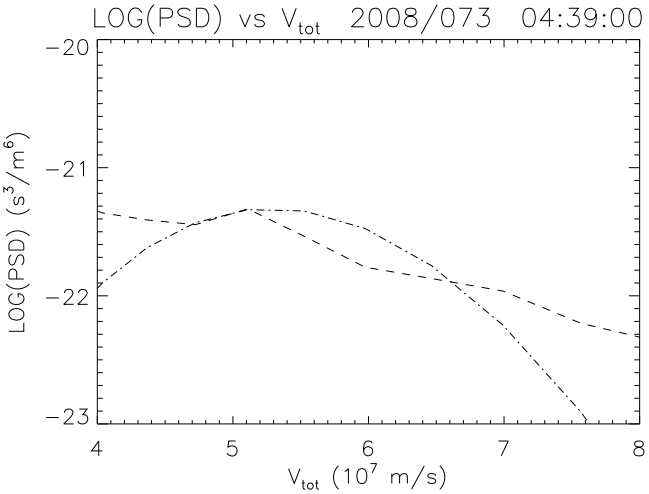

Figure 4. A plot of the data for anode 4 (pitch angle = 88.5°, dashed line) and the Dory-Guest-Harris distribution for the warm component only (dot-dashed line). The curves nearly coincide at $\sim V_{tot} = 5 \times 10^7$ m/s, close to the resonance velocity.

region [cf. *Mutel et al.*, 2010a]. The fit of the model for the shell-like distribution near $V_{tot} = 4$ to 6×10^7 m/s is important to the growth rate calculations in the CMI theory, because it lies near the resonance circle. The cold core distribution (j = 0) is included in the fit, but the observed low-energy plasma contains photoelectrons and trapped electrons owing to spacecraft charging and should not be compared to the model low-energy plasma.

[13] The growth rates for the X mode (and Z mode) and the O mode in the CMI are given in a simple form as

$$\text{X mode } \gamma = \frac{\omega_i}{\Omega_{ce}} = \frac{\pi^2}{4}\frac{n_\omega}{n_e^2}\beta^2 c^2 \nu_r^2 \int_0^\pi d\psi \sin^2\psi \left[\frac{\partial f}{\partial \nu_\perp} + \frac{k_\parallel \nu_\perp}{\Omega_{ce}}\frac{\partial f}{\partial \nu_\parallel}\right]_{|\nu|=\nu_r} \quad (2)$$

$$\text{O mode } \gamma = \frac{\omega_i}{\Omega_{ce}} = \frac{\pi^2}{16}\frac{n_\omega}{n_e^2}\beta^2 \nu_r^4 \int_0^\pi d\psi \sin^2(2\psi) \left[\frac{\partial f}{\partial \nu_\perp} + \frac{k_\parallel \nu_\perp}{\Omega_{ce}}\frac{\partial f}{\partial \nu_\parallel}\right]_{|\nu|=\nu_r} \quad (3)$$

where ω_i is the imaginary part of the angular frequency, n_ω is the density of warm plasma, Ω_{ce} is the electron angular cyclotron frequency, β is the ratio of electron plasma frequency to electron cyclotron frequency, Ψ is the electron pitch angle, and f is the electron distribution function, and $k_\parallel$ is the parallel component of the wave normal vector. The integration path is along the resonance ellipse, which for $v \ll c$ is a circle given by $\nu_r = (\nu_c^2 - 2c^2\delta\omega)^{1/2}$ with $\nu_c = k_\parallel c^2/\Omega_{ce}$ and $\delta_\omega = (\omega - \Omega_{ce})/\Omega_{ce}$. At this time $f_{ce} = 4450$ Hz. Results of growth rate calculations for the X mode are performed for a range of wave normal angles and ratios f/f_{ce} and are displayed in a two-dimensional contour plot in Figure 5a. Strongest growth occurs for wave normal angles extending over 20° and for ratios $0.990 < f/f_{ce} < 0.994$. The stepped nature of the plot results from finite iterations of the parameters. The growth rates are comparable to those determined by *Mutel et al.* [2010a] for the SKR observations on day 291, 2008. Figure 5b displays contours of the growth rate for the Z mode over the range of wave normal angles 86° to 90° and $0.982 < f/f_{ce} < 0.988$. Since the Z mode is a trapped mode and does not propagate for $f > f_{UH}$ (where f_{UH} is the upper hybrid frequency) wave normal angles greater than 90° were not plotted. The Z mode growth rate is robust, comparable to X mode growth. Finally, Figure 5c shows the contours of growth rate for the O mode. These rates are approximately two orders of magnitude lower than those for the X mode, as expected [cf. *Mellott et al.*, 1984; *Lamy et al.*, 2011]. They are shown as a function of wave normal angle both less than and greater than 90°, since these waves can propagate both toward and away from Saturn without immediately encountering a cutoff or resonance. O mode propagates across f_{ce}, and is reflected only near f_p.

[14] Small changes in the DGH distribution function fitting parameters n_w, $V_\parallel$, and $V_\perp$ have a modest effect on the wave growth rate calculations. For example, simultaneously decreasing n_w by 9% and $V_\parallel$ and $V_\perp$ each by 3% produces essentially the same results displayed in Figure 5, but the maximum growth rate for X, Z, and O modes changes by ~6%, ~12%, and ~19%, respectively.

[15] To estimate the power gain of the observations relative to the sky background and to the calculated gain we refer to the discussion in the work of *Mutel et al.* [2010a, section 2.3]. From Figure 1a we note that the intensity of the observed electric fields of the X mode near the source region is $\sim 10^{-11}$ V^2/(m^2 Hz) or equivalently about 1.7×10^{-15} W/(m^2 Hz), and we estimate the background intensity is $\sim 6 \times 10^{-24}$ W/(m^{-2} Hz) [cf. *Mutel et al.*, 2010a], yielding an observed gain of $G_{obs} \sim 3 \times 10^8$. In estimating the gain from the CMI we write $G_{CMI} = \exp[(2\omega_i L_c)/V_g]$, where L_c is the convective growth length assumed to be ~1000 km, and V_g is the group velocity, which we assume to be ~0.1 c [cf. *Winglee*, 1985; *Mutel et al.*, 2010a]. For $\omega_i \sim 0.01$–$0.02\ \Omega_{ce}$ these substitutions yield $G_{CMI} \sim 1.5$–3.0×10^8 which is comparable to the observed gain. The Z mode emission for $f < f_{ce}$ near the source region is indistinguishable from the X mode owing to the low-frequency resolution. Further away from the source region the spectral density varies between $\sim 10^{-11}$ V^2/(m^2 Hz) to $\sim 10^{-13}$ V^2/(m^2 Hz) with a rough period of about 20 min. We speculate this may be due to temporal effects such as changing local plasma conditions within the source region. We note the X mode emission also shows a general burstiness of approximately the same period seen in Figure 1a during the time period 02:00 to 04:00 UT. The ordinary mode emission is observed to be about two orders of magnitude lower in intensity, and consequently the expected gain would be extremely small for comparable values of L_c and V_g. Yet the O mode is observable at an X/O mode intensity ratio of about 100 as it was also for the SKR encounter reported by *Lamy et al.* [2011]. This may indicate that the observed O mode is primarily NB emission or, as shown by *Pritchett and Strangeway* [1985] for the case of

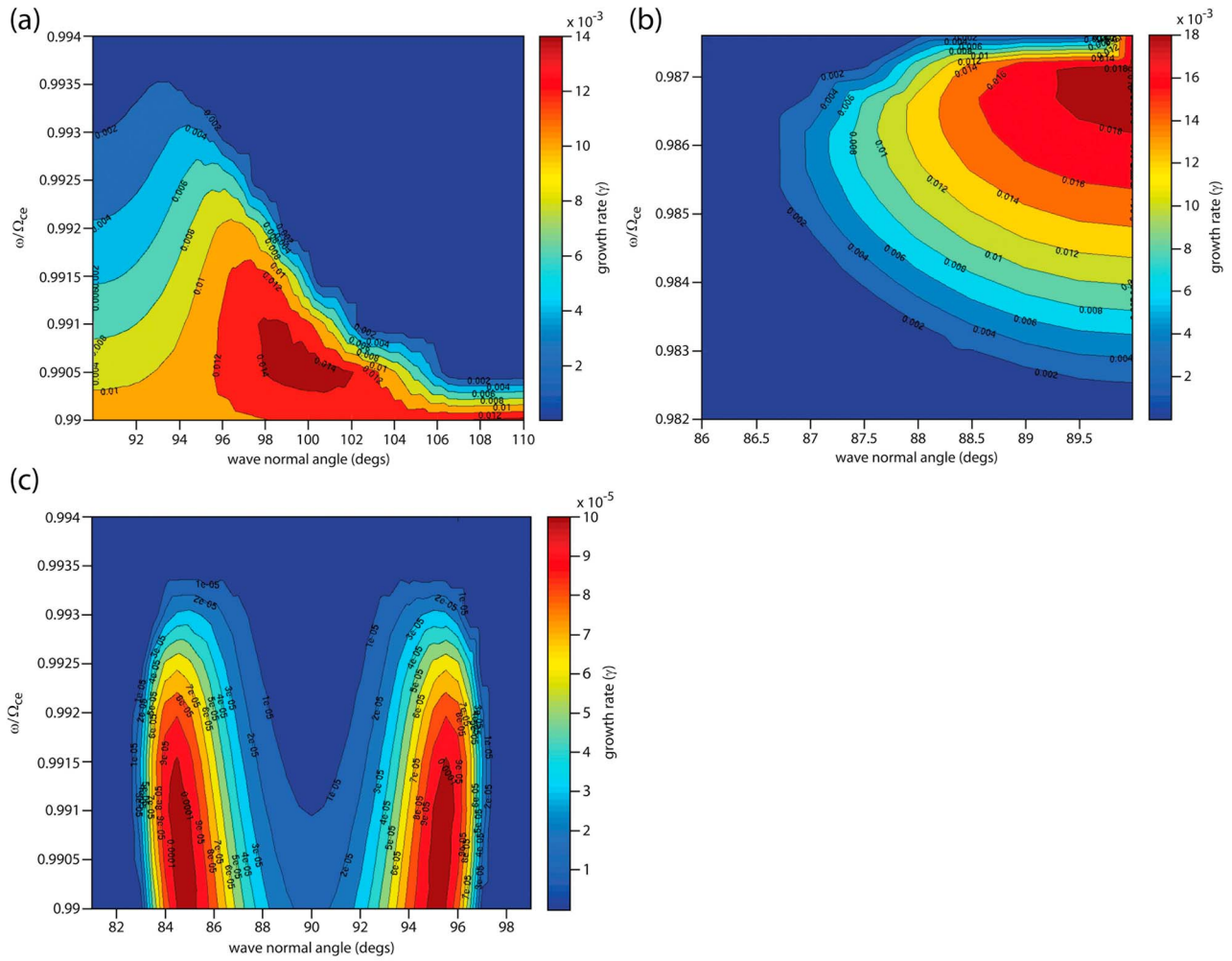

Figure 5. (a) Contours of positive relative growth rate (γ/Ω_c) for the X mode are plotted as a function of normalized frequency and wave normal angle. (b) Same as Figure 5a but for Z mode. (c) Same as Figure 5a but for O mode.

terrestrial AKR, may be due to nonlinear effects as discussed in section 4.

4. Summary and Conclusions

[16] Discovery of a second possible SKR source region [*Menietti et al.*, 2010] has allowed the comparison of observations and an estimate of SKR growth rates. In this study we have extended the original investigation by also examining the O mode and Z mode emissions in addition to the previously studied X mode. Ordinary mode emission has been reported emanating from terrestrial AKR source regions [cf. *Mellott et al.*, 1984; *Bahnsen et al.*, 1989], and was reported by *Lamy et al.* [2011] for the first reported SKR source region. Thus the present observations are consistent with both terrestrial and Saturn source region observations. However, growth rate calculations based on the CMI indicate that the gain for the O mode is much too low to account for observed intensity levels. An alternative explanation is that the observed ordinary mode emission is NB emission, and is not solely from the SKR source region. Nevertheless, *Pritchett and Strangeway* [1985, hereinafter PS] have considered an analogous situation regarding terrestrial auroral O mode observations of *Mellott et al.* [1984]. PS performed relativistic particle-in-cell simulations of AKR along terrestrial auroral field lines using reasonable plasma parameters and found that the calculated O mode electric power was about 1% of the X mode, in agreement with the DE-1 satellite observations of *Mellott et al.* [1984]. For comparison, PS then analytically evaluated the growth rate using the semirelativistic approximation [*Wu and Lee*, 1979; this study] and a DGH distribution for appropriate plasma parameters. They found that the growth rate of O mode emission should be $\lesssim$ 1% that of X mode, and too small to be observable. They concluded that a nonlinear mechanism is responsible for the O mode generation. The wave growth generates relativistic coupling between all three velocity components of an electron in the presence of the perpendicular wave electric fields and the ambient magnetic field, generating a parallel current. This current in turn excites ordinary mode wavefields of ~1% of the X mode and comparable to those observed by *Mellott et al.*

[1984]. The ordinary mode emission at Saturn is observed to be about 1% of the intensity of X mode, so a nonlinear relativistic coupling within the SKR source center may also explain the observed much larger gains (~1% of the X mode intensity) than predicted by the quasi-linear CMI theory.

[17] Some of the Z mode observations reported in this work may be propagating from the SKR source region have not been reported before. While such emission is theoretically possible [cf. *Omidi et al.*, 1984; *Winglee*, 1985], in the past there have not been clear reports of observed Z mode emission distinguished from X mode emission within terrestrial AKR source regions. *Mutel et al.* [2010b] have reported Cluster observations, however, near the AKR source regions that do appear to be distinguished from the X mode. The observations of Z mode reported here may either correspond to NB emission or to CMI-driven emission from the SKR source region, consistent with very recent terrestrial observations.

[18] The wave observations present a brief encounter (several minutes) with an SKR source region at frequencies near 4.5 kHz near a local time of 8 h at a latitude of approximately −50°. This is close to the nominal local time of SKR source regions as reported by *Lamy et al.* [2009]. Interestingly, this region is traversed by NB emission from a probable remote source region and propagating in a frequency range ~6 kHz < f < 7.5 kHz. While this emission, which is known to propagate in O and Z modes, overlays some of the SKR emission, we have presented arguments suggesting that the SKR source region emits in X, O, and Z modes. These arguments include the observation of X, Z, and O mode emission near the source region (04:35–04:40 UT) based on apparent polarization measurements. Intensity levels of the observed X and Z mode emission are comparable to those expected on the basis of growth rate calculations for the measured electron phase space distribution. The higher observed O mode intensity levels may be due to a nonlinear coupling mechanism. Apparent polarization measurements have limitations as discussed in section 3. If one assumes that the NB emission from remote source regions extends to frequencies less than 5 kHz near 04:39 UT then the Z mode emission for $f < f_{ce}$ and O mode emission may be explained by the presence of NB emission alone. The intensity levels of SKR for this event are somewhat smaller than those previously reported for day 291 of 2008 [*Lamy et al.*, 2010]. In addition, the pitch angle coverage of the ELS instrument is not as complete as for the event of day 291, but the observations suggest a shell-like electron distribution centered near 7 keV, somewhat lower than that reported for the day 291 event. On the basis of assumptions outlined above, the modeled electron distribution is adequate to generate X and Z mode emission at the intensity levels similar to the observations. The O mode intensity levels may be explained by nonlinear processes as discussed above.

[19] **Acknowledgments.** Research at the University of Iowa was supported by NASA through contract 1415150 with the Jet Propulsion Laboratory. J.D.M. thanks A. Persoon and J. Chrisinger for their assistance with a number of the figures in this work and J. Barnholdt for clerical assistance. L.L. acknowledges support from CNRS, Observatoire de Paris, and CNES.

[20] Masaki Fujimoto would like to thank two anonymous reviewers for their assistance in evaluating this paper.

References

Bahnsen, A., B. M. Pedersen, M. Jespersen, E. Ungstrup, L. Eliasson, J. S. Murphree, R. D. Elphinstone, L. Blomberg, G. Holmgren, and L. J. Zanetti (1989), Viking observations at the source region of auroral kilometric radiation, *J. Geophys. Res.*, *94*, 6643–6654, doi:10.1029/JA094iA06p06643.

Benson, R. F., P. A. Webb, J. L. Green, D. L. Carpenter, V. S. Sonwalkar, H. G. James, and B. W. Reinisch (2006), Active wave experiments in space plasmas: The Z mode, in *Geospace Electromagnetic Waves and Radiation*, *Lecture Notes Phys.*, vol. 687, edited by James W. LaBelle and Rudolf A. Treumann, pp. 3–35, Springer, Berlin, doi:10.1007/b11580119.

Bunce, E., et al. (2010), Extraordinary field-aligned current signatures in Saturn's high-latitude magnetosphere: Analysis of Cassini data during Revolution 89, *J. Geophys. Res.*, *115*, A10238, doi:10.1029/2010JA015612.

Cecconi, B., and P. Zarka (2005), Direction finding and antenna calibration through analytical inversion of radio measurements performed using a system of two or three electric dipole antennas on a three-axis stabilized spacecraft, *Radio Sci.*, *40*, RS3003, doi:10.1029/2004RS003070.

Cecconi, B., L. Lamy, P. Zarka, R. Prangé, W. S. Kurth, and P. Louarn (2009), Goniopolarimetric study of the revolution 29 perikrone using the Cassini Radio and Plasma Wave Science instrument high-frequency radio receiver, *J. Geophys. Res.*, *114*, A03215, doi:10.1029/2008JA013830.

Delory, G. T., R. E. Ergun, C. W. Carlson, L. Muschietti, C. C. Chaston, W. Peria, J. P. McFadden, and R. Strangeway (1998), FAST observations of electron distributions within AKR source regions, *Geophys. Res. Lett.*, *25*, 2069–2072, doi:10.1029/98GL00705.

Dory, R. A., G. E. Guest, and E. G. Harris (1965), Unstable electrostatic plasma waves propagating perpendicular to a magnetic field, *Phys. Rev. Lett.*, *14*, 131–133, doi:10.1103/PhysRevLett.14.131.

Ergun, R. E., et al. (1998), FAST satellite observations of large-amplitude solitary structures, *Geophys. Res. Lett.*, *25*, 2041–2044, doi:10.1029/98GL00636.

Fischer, G., B. Cecconi, L. Lamy, S.-Y. Ye, U. Taubenschuss, W. Macher, P. Zarka, W. S. Kurth, and D. A. Gurnett (2009), Elliptical polarization of Saturn Kilometric Radiation observed from high latitudes, *J. Geophys. Res.*, *114*, A08216, doi:10.1029/2009JA014176.

Gurnett, D. A., W. S. Kurth, and F. L. Scarf (1981), Narrowband electromagnetic emissions from Saturn's magnetosphere, *Nature*, *292*, 733–737, doi:10.1038/292733a0.

Gurnett, D. A., S. D. Shawhan, and R. R. Shaw (1983), Auroral hiss, Z mode radiation, and auroral kilometric radiation in the polar magnetosphere: DE 1 observations, *J. Geophys. Res.*, *88*, 329–340, doi:10.1029/JA088iA01p00329.

Gurnett, D. A., W. Calvert, R. L. Huff, D. Jones, and M. Sugiura (1988), The polarization of escaping terrestrial continuum radiation, *J. Geophys. Res.*, *93*, 12,817–12,825.

Gurnett, D. A., et al. (2004), The Cassini radio and plasma wave investigation, *Space Sci. Rev.*, *114*, 395–463, doi:10.1007/s11214-004-1434-0.

Jackman, C. M., L. Lamy, M. P. Freeman, P. Zarka, B. Cecconi, W. S. Kurth, S. W. H. Cowley, and M. K. Dougherty (2009), On the character and distribution of lower-frequency radio emissions at Saturn and their relationship to substorm-like events, *J. Geophys. Res.*, *114*, A08211, doi:10.1029/2008JA013997.

Jackman, C. M., C. S. Arridge, J. A. Slavin, S. E. Milan, L. Lamy, M. K. Dougherty, and A. J. Coates (2010), In situ observations of the effect of a solar wind compression on Saturn's magnetotail, *J. Geophys. Res.*, *115*, A10240, doi:10.1029/2010JA015312.

Jones, D. (1976), Source of terrestrial non-thermal radiation, *Nature*, *260*, 686–689, doi:10.1038/260686a0.

Kurth, W. S., et al. (2005), An Earth-like correspondence between Saturn's auroral features and radio emission, *Nature*, *433*, 722–725, doi:10.1038/nature03334.

Kurth, W. S., et al. (2010), A close encounter with a Saturn kilometric radiation source region, paper presented at 7th International Workshop on Planetary, Solar, and Heliospheric Radio Emissions, Austrian Acad. of Sci., Graz, Austria.

Lamy, L., P. Zarka, B. Cecconi, R. Prangé, W. S. Kurth, and D. A. Gurnett (2008), Saturn kilometric radiation: Average and statistical properties, *J. Geophys. Res.*, *113*, A07201, doi:10.1029/2007JA012900.

Lamy, L., B. Cecconi, R. Prangé, P. Zarka, J. D. Nichols, and J. T. Clarke (2009), An auroral oval at the footprint of Saturn's kilometric radio sources, colocated with the UV aurorae, *J. Geophys. Res.*, *114*, A10212, doi:10.1029/2009JA014401.

Lamy, L., et al. (2010), Properties of Saturn kilometric radiation measured within its source region, *Geophys. Res. Lett.*, *37*, L12104, doi:10.1029/2010GL043415.

Lamy, L., B. Cecconi, P. Zarka, P. Canu, P. Schippers, W. S. Kurth, R. L. Mutel, D. A. Gurnett, D. Menietti, and P. Louarn (2011), Emission

and propagation of Saturn kilometric radiation: Magnetoionic modes, beaming pattern, and polarization state, *J. Geophys. Res.*, *116*, A04212, doi:10.1029/2010JA016195.

Louarn, P., and D. Le Queau (1996), Generation of the auroral kilometric radiation in plasma cavities—II. The cyclotron maser instability in small size sources, *Planet. Space Sci.*, *44*, 211–224, doi:10.1016/0032-0633(95)00122-0.

Louarn, P., et al. (2007), Observations of similar radio signatures at Saturn and Jupiter: Implications for the magnetospheric dynamics, *Geophys. Res. Lett.*, *34*, L20113, doi:10.1029/2007GL030368.

Mellott, M. M., W. Calvert, R. L. Huff, D. A. Gurnett, and S. D. Shawhan (1984), DE-1 observations of ordinary mode and extraordinary mode auroral kilometric radiation, *Geophys. Res. Lett.*, *11*, 1188–1191, doi:10.1029/GL011i012p01188.

Melrose, D. B. (1981), A theory for the nonthermal radio continua in the terrestrial and Jovian magnetospheres, *J. Geophys. Res.*, *86*, 30–36, doi:10.1029/JA086iA01p00030.

Menietti, J. D., R. L. Mutel, P. Schippers, S.-Y. Ye, O. Santolik, W. S. Kurth, D. A. Gurnett, L. Lamy, and B. Cecconi (2010), Saturn kilometric radiation near a source center on day 73, 2008, paper presented at 7th International Workshop on Planetary, Solar, and Heliospheric Radio Emissions, Austrian Acad. of Sci., Graz, Austria.

Mutel, R. L., J. D. Menietti, D. A. Gurnett, W. Kurth, P. Schippers, C. Lynch, L. Lamy, C. Arridge, and B. Cecconi (2010a), CMI growth rates for Saturnian kilometric radiation, *Geophys. Res. Lett.*, *37*, L19105, doi:10.1029/2010GL044940.

Mutel, R. L., I. Christopher, J. Menietti, D. Gurnett, J. Pickett, A. Masson, A. Fazakerley, and E. Lujek (2010b), X and Z mode growth rates and propagation at cavity boundaries, paper presented at 7th International Workshop on Planetary, Solar, and Heliospheric Radio Emissions, Austrian Acad. of Sci., Graz, Austria.

Omidi, N., C. S. Wu, and D. A. Gurnett (1984), Generation of auroral kilometric and Z mode radiation by the cyclotron maser mechanism, *J. Geophys. Res.*, *89*, 883–895, doi:10.1029/JA089iA02p00883.

Pritchett, P. L., and R. J. Strangeway (1985), A simulation study of kilometric radiation generation along an auroral field line, *J. Geophys. Res.*, *90*, 9650–9662, doi:10.1029/JA090iA10p09650.

Pritchett, P. L., R. J. Strangeway, R. E. Ergun, and C. W. Carlson (2002), Generation and propagation of cyclotron maser emissions in the finite auroral kilometric radiation source cavity, *J. Geophys. Res.*, *107*(A12), 1437, doi:10.1029/2002JA009403.

Schippers, P., et al. (2011), Auroral electron distributions within and close to the Saturn kilometric radiation source region, *J. Geophys. Res.*, *116*, A05203, doi:10.1029/2011JA016461.

Su, Y.-J., R. E. Ergun, S. T. Jones, R. J. Strangeway, C. C. Chaston, S. E. Parker, and J. L. Horwitz (2007), Generation of short-burst radiation through Alfvénic acceleration of auroral electrons, *J. Geophys. Res.*, *112*, A06209, doi:10.1029/2006JA012131.

Wang, Z., D. A. Gurnett, G. Fischer, S.-Y. Ye, W. S. Kurth, D. G. Mitchell, J. S. Leisner, and C. T. Russell (2010), Cassini observations of narrowband radio emissions in Saturn's magnetosphere, *J. Geophys. Res.*, *115*, A06213, doi:10.1029/2009JA014847.

Warwick, J. W., et al. (1981), Planetary radio astronomy observations from Voyager 1 near Saturn, *Science*, *212*, 239–243, doi:10.1126/science.212.4491.239.

Winglee, R. M., (1985), Fundamental and harmonic electron cyclotron maser emission, *J. Geophys. Res.*, *90*, 9663–9674, doi:10.1029/JA090iA10p09663.

Wu, C. S., and L. C. Lee (1979), A theory of terrestrial kilometric radiation, *Astrophys. J.*, *230*, 621–626, doi:10.1086/157120.

Ye, S.-Y., D. A. Gurnett, G. Fischer, B. Cecconi, J. D. Menietti, W. S. Kurth, Z. Wang, G. B. Hospodarsky, P. Zarka, and A. Lecacheux (2009), Source locations of narrowband radio emissions detected at Saturn, *J. Geophys. Res.*, *114*, A06219, doi:10.1029/2008JA013855.

Ye, S.-Y., J. D. Menietti, G. Fischer, Z. Wang, B. Cecconi, D. A. Gurnett, and W. S. Kurth (2010), Z mode waves as the source of Saturn narrowband radio emissions, *J. Geophys. Res.*, *115*, A08228, doi:10.1029/2009JA015167.

Young, D. T., et al. (2004), Cassini plasma spectrometer investigation, *Space Sci. Rev.*, *114*, 1–112, doi:10.1007/s11214-004-1406-4.

Zarka, P. (1998), Auroral radio emissions at the outer planets: Observations and theories, *J. Geophys. Res.*, *103*, 20,159–20,194.

D. A. Gurnett, J. D. Menietti, R. L. Mutel, P. Schippers, and S.-Y. Ye, Department of Physics and Astronomy, University of Iowa, 210 Van Allen Hall, Iowa City, IA 52242-1479, USA. (donald-gurnett@uiowa.edu; john-menietti@uiowa.edu; robert-mutel@uiowa.edu; patricia-schippers@uiowa.edu; shengyi-ye@uiowa.edu)

L. Lamy, LESIA, Observatoire de Paris, Université Paris Diderot, UPMC, CNRS, 5 Place Jules Janssen, F-92195 Meudon, France. (laurent.lamy@obspm.fr)